



# Using numerical simulations to compare the fracture toughness values for concrete from the size-effect, two-parameter and fictitious crack models

James H. Hanson <sup>a,\*</sup>, Anthony R. Ingraffea <sup>b</sup>

<sup>a</sup> Department of Civil Engineering, Rose-Hulman Institute of Technology, 5500 Wabash Avenue, Terre Haute, IN 47803, USA

<sup>b</sup> School of Civil and Environmental Engineering, Cornell University, 220 Hollister Hall, Ithaca, NY 14853, USA

---

## Abstract

The size-effect, two-parameter, and fictitious crack models were developed to predict crack growth in materials like concrete that experience tension softening. The three models must predict the same response for infinitely large structures. Therefore, this study evaluates the differences in response for smaller structures. The metric used to compare response is the fracture toughness value required by the model to generate a particular load versus crack mouth opening displacement graph for a single edge specimen loaded in bending. The graphs, including unloading response, were generated numerically using the fictitious crack model and seventeen different sets of property values. The size-effect and two-parameter data reduction methods were then applied to the graphs to determine the associated fracture toughness values. Results of the evaluation indicate that the fracture toughness values for the size-effect and two-parameter models tend to be less than those of the fictitious crack model. However, there is a range of simulated materials for which the models are in reasonable agreement for structures on the scale of standard laboratory specimens.

© 2002 Elsevier Science Ltd. All rights reserved.

*Keywords:* Fracture toughness; Concrete; Size-effect model; Two-parameter model; Fictitious crack model; Cohesive crack simulation; Data reduction methods

---

## 1. Introduction

The size-effect [1], two-parameter [2] and fictitious crack [3] models were developed to account for non-linear fracture mechanics (NLFM) conditions when predicting crack growth in materials like concrete that experience tension softening ahead of an advancing crack. Elices and Planas [4] compared the three models and showed that the models predict the same behavior only for a limited range of structure sizes. For infinitely large structures, the tension softening zone (TSZ) is negligibly small; therefore, the crack experiences linear elastic fracture mechanics (LEFM) conditions. Each of the models was developed such that it is consistent with LEFM for infinitely large structures. Rather than match behaviors at some finite structure

---

\* Corresponding author. Fax: +1-812-877-8440.

E-mail address: [jh87@cornell.edu](mailto:jh87@cornell.edu) (J.H. Hanson).

size and observe differences in behavior for infinitely large structures, this study asserts that the models should all predict the same behavior for infinitely large structures and compares differences in behavior for a range of finite structure sizes.

In order to quantitatively compare response of a structure using each of the crack propagation models, the authors chose to compare the fracture toughness value required by each model to generate a particular structural response. The structural response chosen was the load versus crack mouth opening displacement (CMOD) of a single edge specimen loaded in bending. Graphs of the response were generated using numerical simulations based on the fictitious crack model, and assuming a wide range of TSZ property values in this model. The simulated response included unloading response. The size-effect [5] and two-parameter [6] data reduction methods were applied to the data in the graphs in order to determine the fracture toughness values required by the models to generate the same response.

The scope of this investigation was not limited to TSZ property values for common concretes. The scope was developed to compare the models over a wide range of TSZ property values. Therefore, as new concretes are developed, the results of this study will still provide insight into how the models will compare when predicting behavior of structures made from such materials.

### 1.1. Structure geometry

The structure chosen for this investigation is the single edge specimen loaded in bending, SE(B), a standard fracture toughness test specimen. Three sizes of SE(B) were simulated for each set of TSZ property values. The dimensions conform to the requirements of two proposed testing standards through the RILEM organization [5,6]. The details of the specimen geometries are shown in Fig. 1. The total ligament length is the distance  $W - a_o$ , which equals  $0.67W$  for all three specimen sizes. The supports were simulated as lines of constrained vertical displacement. The loaded region was  $3.2 \text{ mm} \times 79 \text{ mm}$  for all three specimen sizes.

### 1.2. Simulation tools

The simulation program used in this study was CohFRANC3D, which was developed and is maintained by the Cornell Fracture Group, <http://www.cfg.cornell.edu> [7–10]. The program uses the dual boundary element method (BEM) to analyze fully three-dimensional models. The model used for the smallest SE(B) is shown in Fig. 2.

The CohFRANC3D program implements the fictitious crack model numerically using influence coefficients [8,11]. The program was used to generate simulated load versus CMOD responses for the SE(B)

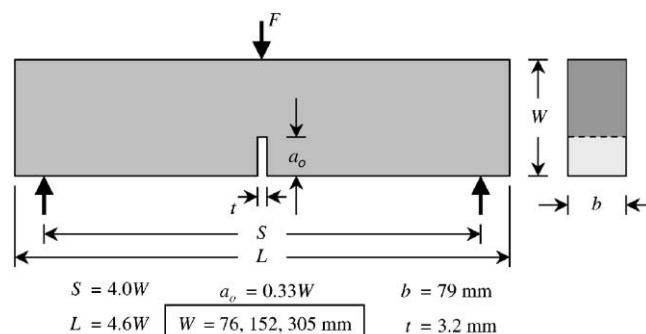


Fig. 1. Single edge specimen loaded in bending. Dimensions are for the three simulated test specimen geometries.

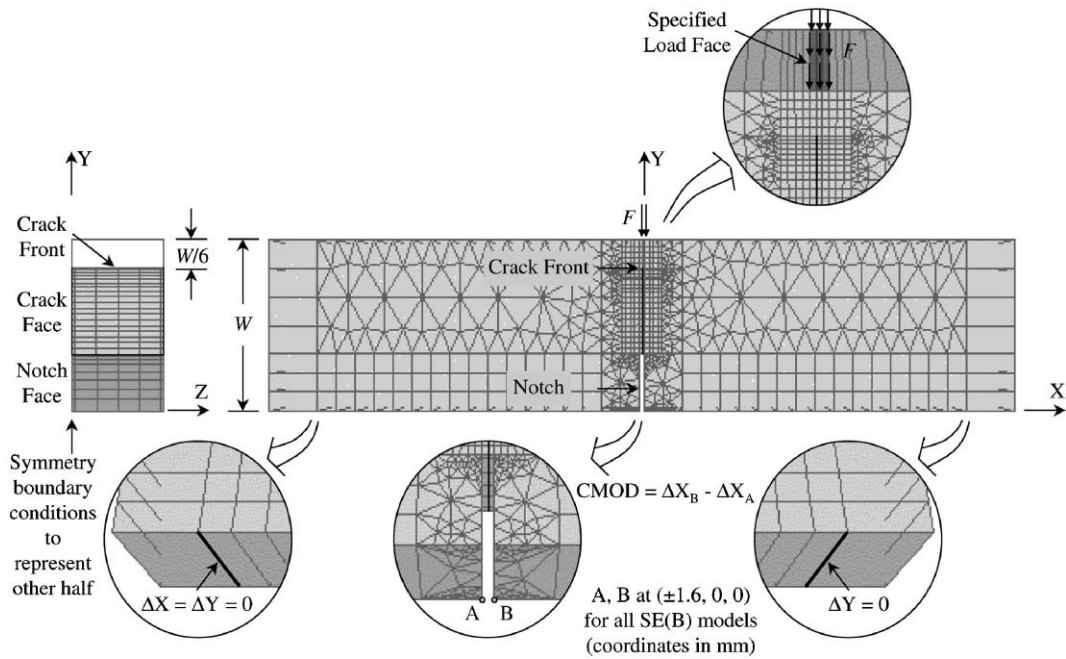


Fig. 2. BEM model used to simulate the 76 mm deep SE(B) specimens.

structures. The simulation capabilities do not permit the cohesive crack to extend through the entire height of the simulated specimen; therefore, the extent of the simulated load versus CMOD response is limited. The program also utilizes the focal point model by Yankelevsky and Reinhardt [12] to predict the unloading response of a structure after the simulated process zone begins to grow. A schematic of the focal point model is presented in Fig. 3. An example of a simulated response of a specimen with  $W = 76$  mm is shown in Fig. 4. Based on detailed studies [10], inaccuracies in the simulated load versus CMOD data points are in the range of 5–15% due to approximations in the BEM generated influence coefficients.

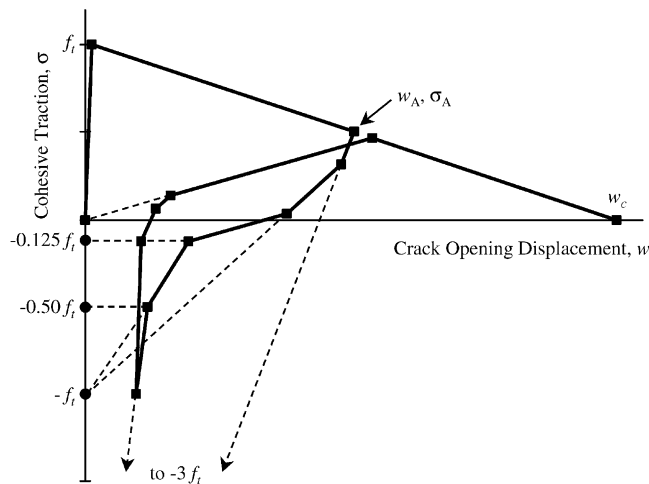


Fig. 3. Schematic representation of the focal point model used to predict unloading response of concrete in the TSZ.

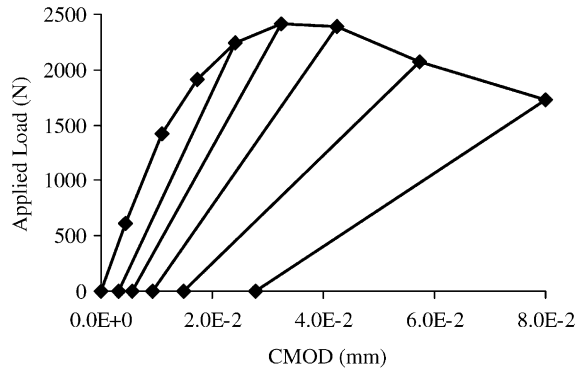


Fig. 4. Typical simulated load versus CMOD response of a 76 mm deep SE(B) specimen including unload cycles.

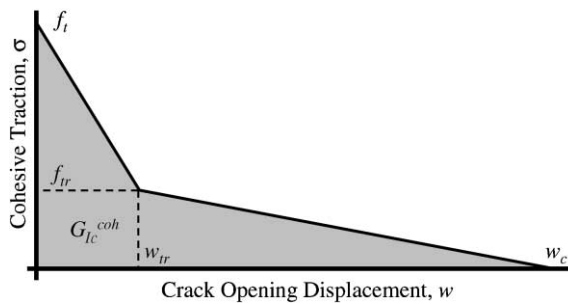


Fig. 5. Bilinear TSD used to govern the stress versus COD behavior of a simulated specimen during a cohesive crack simulation.

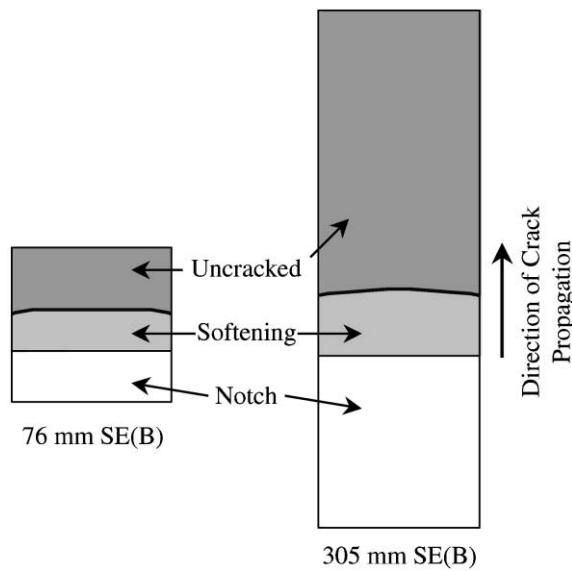


Fig. 6. Simulated crack profiles at peak load of 76 and 305 mm deep SE(B) specimens for TSD series A (refer to Table 1 for information on TSD series A).

For the fictitious crack model, the TSZ properties of the material are characterized by the tension softening diagram (TSD) Fig. 5. The TSD is a constitutive relationship that governs the stress versus crack opening displacement (COD) behavior of the material. The CohFRANC3D program accepts TSD parameters for either linear or bilinear softening.

The SE(B) structures were modeled in three dimensions in order to allow for any through thickness variation in crack length during the simulated tests. Swartz and Go noted a significant such variation in laboratory tests of concrete SE(B) structures [13]. The simulated crack profiles from this study support their observations. For example, plots of a typical crack profile at peak load for the smallest and largest SE(B) for one set of TSZ property values is presented in Fig. 6. These show the demarcation between uncracked and softening regions where the tensile stress has reached the limit value,  $f_t$ . The crack profiles agree with the observations of Swartz and Go [13] except that the simulated SE(B) structures do not demonstrate a sudden increase of crack length near the free surfaces. This observed phenomena from the laboratory tests is likely due to shrinkage cracking which was not reproduced in the simulations.

## 2. Crack propagation models

### 2.1. Size-effect model

The size-effect model [1] defines the nominal strength,  $\sigma_N$ , as the peak load divided by two structure dimensions. Therefore,  $\sigma_N$  can be related to the size-dependent fracture energy,  $G_{IQ}$ , by Eq. (1) where,  $F_{max}$  is the peak load,  $E$  is the modulus of elasticity, and  $g(\alpha_o)$  is a geometry function that depends on shape, boundary conditions and relative crack length,  $\alpha_o$ . Eq. (1) can be algebraically manipulated to obtain an expression for  $G_{IQ}$  (Eq. (2)):

$$\left(\frac{F_{max}}{bW}\right)^2 = \sigma_N^2 = \frac{G_{IQ}E}{Wg(\alpha_o)} \tag{1}$$

$$G_{IQ} = \frac{Wg(\alpha_o)}{(1/\sigma_N^2)E} \tag{2}$$

The size-effect model assumes that the nominal strength of geometrically similar structures is only a function of one structure dimension, say  $W$ . The relationship proposed by Bazant [14] is given in Eq. (3) where  $Bf'_t$  and  $\lambda_o d_a$  are constants for a given material as defined in [1]. Eq. (3) can be algebraically manipulated to obtain Eq. (4) which is in the form  $y = Ax + D$ . Therefore, the constants can be found by conducting linear regression of the  $1/\sigma_N^2$  versus  $W$  data for several structure sizes:

$$\sigma_N^2 = \frac{(Bf'_t)^2}{1 + \frac{W}{\lambda_o d_a}} \tag{3}$$

$$\frac{1}{\sigma_N^2} = \frac{1}{\lambda_o d_a (Bf'_t)^2} W + \frac{1}{(Bf'_t)^2} \tag{4}$$

Substituting  $A$  and  $D$  into Eq. (4) and combining with Eq. (2) results in a new form of the expression for  $G_{IQ}$  which is still dependent upon the size of the specimen (Eq. (5)). For very large specimens such that  $AW \gg D$ , Eq. (5) reduces to Eq. (6) where  $G_{Ic}^{SZ}$  and  $K_{Ic}^{SZ}$  are fracture energy and fracture toughness, respectively, for infinitely large structures. Data reduction based on the size-effect model is demonstrated in [5]:

$$G_{IQ} = \frac{Wg(\alpha_o)}{(AW + D)E} \tag{5}$$

$$G_{Ic}^{SZ} = \frac{g(\alpha_o)}{AE} \quad \text{or} \quad K_{Ic}^{SZ} = \sqrt{\frac{g(\alpha_o)}{A}} \tag{6}$$

### 2.2. Two-parameter model

The LEFM model for crack growth can be summarized by a relationship between the size-independent fracture toughness,  $K_{Ic}$ , the load applied to the structure when a crack begins to propagate,  $F_{max}$ , and a geometry factor,  $f_1()$ , that considers shape, boundary conditions, and crack length,  $a_c$ , (Eq. (7)):

$$K_{Ic} = F_{max} \times f_1(a_c, \text{geometry, boundary conditions}) \tag{7}$$

The two-parameter model for crack propagation [2] asserts that the global response of a structure with a crack experiencing NLFM conditions can be reproduced by considering the structure to have an effective crack experiencing LEFM conditions. This can be expressed by substituting the effective critical crack length,  $a_c^e$ , into Eq. (7) to obtain Eq. (8):

$$K_{Ic}^{TP} = F_{max} \times f_1(a_c^e, \text{geometry, boundary conditions}) \tag{8}$$

In order to determine the fracture toughness associated with the two-parameter model,  $K_{Ic}^{TP}$ , the effective critical crack length must be obtained. The two-parameter data reduction method [6] uses the unloading compliance of CMOD at peak load,  $C_u$ . Compliance is the inverse of the slope of the unloading curve expressed in displacement per unit load. The compliance is related to the crack length by the relationship in Eq. (9) where  $E$  is the modulus of elasticity of the structure and  $f_2()$  is a geometry function different from  $f_1()$ . Therefore,  $K_{Ic}^{TP}$  can be calculated from the peak load and the compliance at peak load:

$$C_u = \frac{1}{E} \times f_2(a_c^e, \text{geometry, boundary conditions}) \tag{9}$$

### 2.3. Fictitious crack model

The fictitious crack model [3] asserts that, after the stress ahead of a crack reaches a limiting value,  $f_t$ , the material becomes damaged. This damaged material can still transfer stress across the crack path, but the magnitude of stress transferred decreases as the material separates. The fictitious crack model represents the damaged material as a fictitious extension of the stress-free crack. A crack propagating according to the fictitious crack model is shown schematically in Fig. 7.

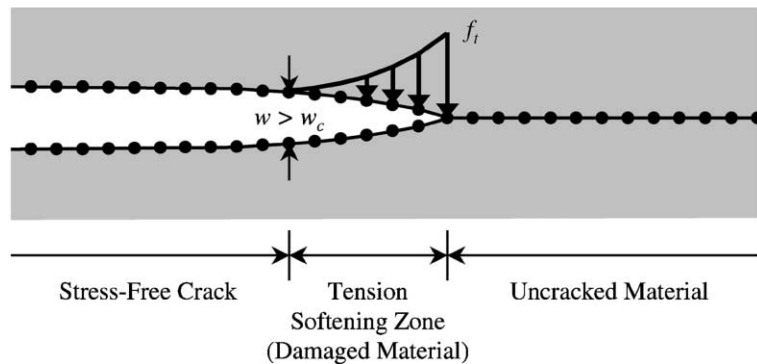


Fig. 7. Schematic representation of a cohesive crack propagating according to the fictitious crack model.

The stress transferred across the fictitious crack is often called a cohesive stress and is expressed as a function of the crack opening in the fictitious crack (Eq. (10)) where  $\sigma$  is the cohesive stress and  $w$  is the COD. The graphical representation of Eq. (10) is the TSD. Several shapes for the function,  $f()$ , including linear [3], bilinear [15], poly-linear [16] and exponential [17], have been used to represent concrete. However, only linear and bilinear (Fig. 6) TSD's have been used in this study:

$$\sigma = f(w) \quad (10)$$

The fracture energy,  $G_{\text{lc}}^{\text{coh}}$ , is the area under the TSD. Using the modulus of elasticity of the simulation model,  $E$ , the fracture energy can be converted to the fracture toughness,  $K_{\text{lc}}^{\text{coh}}$ , where the effect of Poisson's ratio,  $\mu$ , for plane strain conditions is neglected (Eq. (11)):

$$K_{\text{lc}}^{\text{coh}} = \sqrt{\frac{G_{\text{lc}}^{\text{coh}} E}{1 - \mu^2}} \approx \sqrt{G_{\text{lc}}^{\text{coh}} E} \quad (11)$$

### 3. Properties of simulated concretes

#### 3.1. Design of experiments

The scope of this study was developed to compare the three crack propagation models over a wide range of TSZ property values. Therefore, the results of this study might still be used for new concretes with property values outside the range for traditional concretes. In order to represent a broad range of concretes, all of the TSZ properties should be varied. An efficient method for selecting the property values to consider is “design of experiments.”

Design of experiments is a methodology for finding relationships between factors and outputs in a complicated process. In this study, the “factors” are the TSZ properties, the “outputs” are the fracture toughness values for the size-effect and two-parameter models, and the “process” is the numerical simulation of SE(B) response and the application of the respective data reduction method. There are several approaches to design of experiments [18]. For this study, a factorial design was chosen.

Montgomery [18] considers factorial design to be the ideal approach to use when little is known about the behavior of the process and two or more of the factors might interact. The first step is to identify the range of values for each factor. The limits of each range are used in the experiments. This approach uses every possible combination of the limiting values of the factors. The results of the experiments can then be used to predict the optimum values of the factors to achieve the desired output.

#### 3.2. Selection of tension softening diagram property values

A bilinear TSD can be characterized by more than 10 different parameters, but only four are independent. Therefore, the factorial design for this process requires  $2^4 = 16$  evaluations. The factor values can be considered coordinates of the corners of a four-dimensional box surrounding the optimum solution. The center of the box is the seventeenth point evaluated and is added to provide more information about the interactions of the parameters.

The authors chose  $f_t$ ,  $K_{\text{lc}}^{\text{coh}}$ , and the relative location of the transition point,  $f_{\text{tr}}/f_t$  and  $w_{\text{tr}}/w_c$ , as the independent parameters (Fig. 8). The terms  $f_{\text{tr}}$  and  $w_{\text{tr}}$  are the cohesive traction and COD corresponding to the transition point of the bilinear TSD. From these parameters, the characteristic COD where the cohesive traction becomes zero,  $w_c$ , can be determined by Eq. (12).

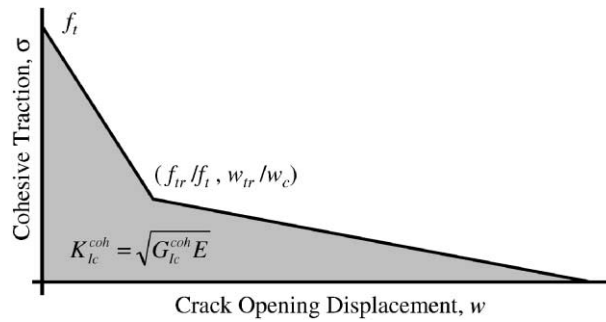


Fig. 8. Bilinear TSD uniquely defined by four independent parameters: tensile limit value,  $f_t$ , cohesive fracture toughness,  $K_{Ic}^{coh}$ , and relative location of the transition point,  $f_{tr}/f_t$  and  $w_{tr}/w_c$ .

Table 1  
Cohesive zone properties used to simulate a variety of concrete mixes

TSD series	Independent parameters				Dependent parameters		
	$f_t$ (MPa)	$K_{Ic}^{coh}$ (MPa $\sqrt{m}$ )	$f_{tr}/f_t$	$w_{tr}/w_c$	$f_{tr}$ (MPa)	$w_{tr}$ (mm)	$w_c$ (mm)
A	2.17	1.10	0.10	0.05	0.22	1.34E-2	2.69E-1
B	2.17	1.10	0.50	0.05	1.09	3.67E-3	7.33E-2
C	2.17	1.10	0.10	0.50	0.22	3.36E-2	6.72E-2
D	2.17	1.10	0.50	0.50	1.09	2.02E-2	4.03E-2
E	2.17	4.40	0.10	0.05	0.22	2.15E-1	4.30E+0
F	2.17	4.40	0.50	0.05	1.09	5.86E-2	1.17E+0
G	2.17	4.40	0.10	0.50	0.22	5.38E-1	1.08E+0
H	2.17	4.40	0.50	0.50	1.09	3.23E-1	6.45E-1
I	9.31	1.10	0.10	0.05	0.93	3.14E-3	6.27E-2
J	9.31	1.10	0.50	0.05	4.65	8.59E-4	1.72E-2
K	9.31	1.10	0.10	0.50	0.93	7.85E-3	1.57E-2
L	9.31	1.10	0.50	0.50	4.65	4.72E-3	9.45E-3
M	9.31	4.40	0.10	0.05	0.93	5.02E-2	1.00E+0
N	9.31	4.40	0.50	0.05	4.65	1.37E-2	2.74E-1
O	9.31	4.40	0.10	0.50	0.93	1.25E-1	2.51E-1
P	9.31	4.40	0.50	0.50	4.65	7.53E-2	1.51E-1
Q	5.74	2.75	0.30	0.28	1.72	4.56E-2	1.66E-1

$$w_c = \frac{2(K_{Ic}^{coh})^2}{f_t E [(f_{tr}/f_t) + (w_{tr}/w_c)]} \quad (12)$$

The range of values of the factors defines the corners of the box. The chosen values are presented in Table 1. The range for  $f_t$  was chosen to be 0.7–3 times the average splitting tensile strength,  $f_s$ , for concrete cast for a laboratory study [10], 3.10 MPa. The range for  $K_{Ic}^{coh}$  was chosen to be 1–4 times an approximate lower bound on the fracture toughness test results from the same laboratory study, 1.1 MPa  $\sqrt{m}$ . The ranges for  $f_{tr}/f_t$  and  $w_{tr}/w_c$  were chosen as 0.10–0.50 and 0.05–0.50, respectively. When the relative transition point is (0.50, 0.50), the TSD is linear. The parameters for the center of the box were defined as the average of the range of each parameter.

The factorial approach to design of experiments resulted in five distinct shapes of TSD's (Fig. 9). The shapes have been normalized such that cohesive traction,  $\sigma$ , is divided by the tensile limit,  $f_t$ , and the COD,

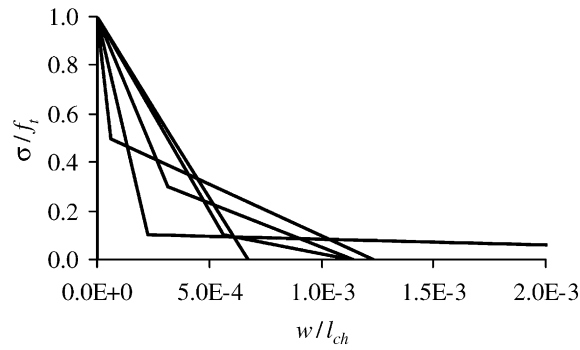


Fig. 9. Family of shapes of TSDs used in this investigation.

$w$ , is divided by the characteristic length,  $l_{ch}$ , defined by Eq. (13). All of the simulated specimens used a modulus of elasticity of 27.6 GPa:

$$l_{ch} = \frac{G_{lc}^{coh} E}{f_t^2} \tag{13}$$

### 4. Results

#### 4.1. Results using the two-parameter model

The results from applying the two-parameter data reduction method [6] to data from all three sizes of SE(B) specimens are presented in Table 2. For some combinations of TSD properties and SE(B) size, the

Table 2  
Results from applying the two-parameter data reduction method to simulated results from three sizes of SE(B) specimens using a variety of TSDs

TSD series	$K_{lc}^{coh}$ input (MPa $\sqrt{m}$ )	$K_{lc}^{TP}$ (MPa $\sqrt{m}$ )			Difference percentage (Eq. (14))			Relative length of TSZ (%) (Eq. (15))		
		76 mm	152 mm	305 mm	76 mm	152 mm	305 mm	76 mm	152 mm	305 mm
A	1.10	0.51	0.59	0.69	-54	-46	-38	40	30	20
B	1.10	0.51	0.68	0.82	-54	-38	-26	50	50	40
C	<b>1.10</b>	0.67	0.80	<b>0.95</b>	-39	-28	<b>-13</b>	50	40	<b>30</b>
D	<b>1.10</b>	0.67	0.81	<b>0.97</b>	-39	-27	<b>-12</b>	50	40	<b>30</b>
E	4.40	-	-	1.92	-	-	-56	$\geq 75$	$\geq 75$	60
F	4.40	-	1.27	1.49	-	-71	-66	$\geq 75$	75	50
G	4.40	-	-	-	-	-	-	$\geq 75$	$\geq 75$	$\geq 75$
H	4.40	-	-	-	-	-	-	$\geq 75$	$\geq 75$	$\geq 75$
I	1.10	0.67	0.91	1.34	-39	-17	22	10	10	10
J	<b>1.10</b>	<b>0.96</b>	<b>1.10</b>	1.43	<b>-13</b>	<b>1</b>	30	<b>20</b>	<b>10</b>	5
K	<b>1.10</b>	<b>0.95</b>	<b>1.12</b>	1.30	<b>-14</b>	<b>2</b>	18	<b>10</b>	<b>10</b>	5
L	<b>1.10</b>	<b>0.96</b>	<b>1.14</b>	<b>1.27</b>	<b>-12</b>	<b>4</b>	<b>15</b>	<b>10</b>	<b>5</b>	<b>5</b>
M	4.40	2.13	2.46	2.80	-51	-44	-36	40	30	20
N	4.40	2.12	2.84	3.44	-52	-35	-22	50	50	40
O	<b>4.40</b>	2.81	3.34	<b>3.98</b>	-36	-24	-9	50	40	<b>30</b>
P	<b>4.40</b>	2.84	3.38	<b>4.04</b>	-35	-23	<b>-8</b>	50	40	<b>30</b>
Q	2.75	1.66	1.94	2.28	-40	-30	-17	50	40	30

Bold entries denote a difference percentage within 15%.

last simulated data point had the largest applied load. As a result, the peak load is not known for sure for those simulated tests. In those cases, the measured fracture toughness,  $K_{Ic}^{TP}$ , of the simulated tests could not be calculated and is omitted from the table.

The objective of comparing the two-parameter and fictitious crack models is to determine whether they predict the same behavior of a concrete structure at the scale of laboratory specimens for some range of cohesive zone property values. Rather than try to quantify closeness of predicted response, the authors chose to quantify the difference in fracture toughness values required to make the same behavior prediction. The comparison of fracture toughness values is expressed as the percentage difference between the output  $K_{Ic}^{TP}$  and the input cohesive fracture toughness,  $K_{Ic}^{coh}$ , for the particular TSD (Eq. (14)). Due to inaccuracies in the simulated load versus CMOD data points and variability of laboratory measured properties of concrete, the authors consider agreement between  $K_{Ic}^{TP}$  and  $K_{Ic}^{coh}$  within 15% as reasonable. Combinations of TSD and SE(B) size that produce reasonable agreement between  $K_{Ic}^{TP}$  and  $K_{Ic}^{coh}$  are highlighted in Table 2. The existence of some combinations of TSD and SE(B) size that produce reasonable agreement of fracture toughness values indicates that there is a range of concretes considered in this study for which the two-parameter and fictitious crack models make reasonably similar predictions of the behavior of laboratory size structures using the same fracture toughness value in each model:

$$\%Diff = \frac{K_{Ic}^{TP \text{ or } SZ} - K_{Ic}^{coh}}{K_{Ic}^{coh}} \quad (14)$$

The relative size length of the TSZ when the peak load occurs is expressed as a percentage of the total ligament length (Eq. (15)). An example of the stress distribution and length of the TSZ is presented in Fig. 10. The ratio of measured fracture toughness to cohesive fracture toughness,  $K_{Ic}^{TP}/K_{Ic}^{coh}$ , is compared to the TSZ percentage length in Fig. 11. For all TSD series, the ratio increased with increasing specimen depth:

$$TSZ\% = \frac{L_{TSZ}}{0.67W} \quad (15)$$

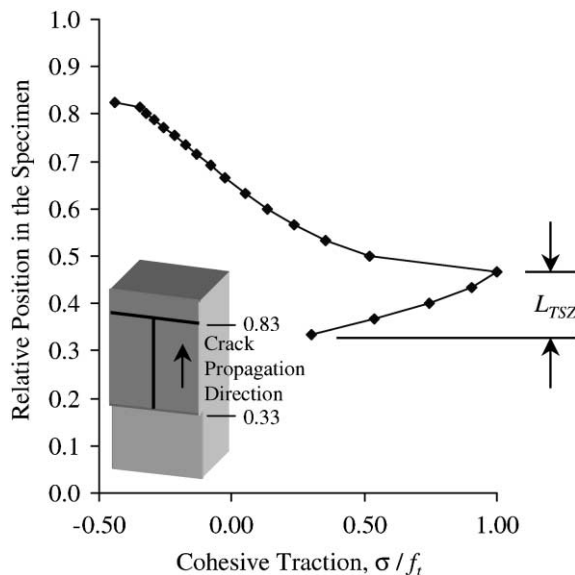


Fig. 10. Distribution of stress in and ahead of the TSZ at peak load in a simulated 305 mm deep SE(B) specimen for TSD series A (refer to Table 1 for information on TSD series A).

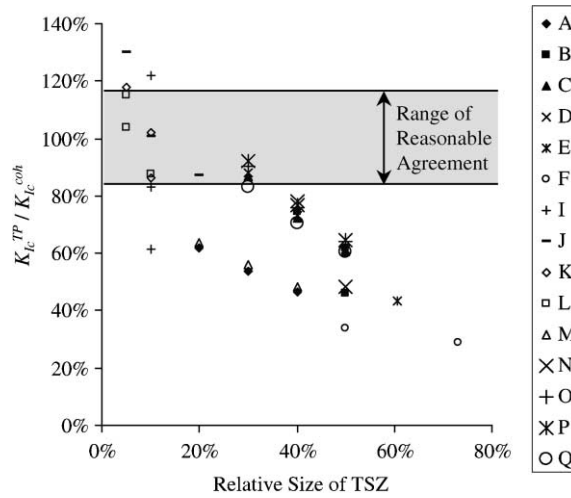


Fig. 11. Plot of the ratio of measured fracture toughness using the two-parameter data reduction method to cohesive fracture toughness as a function of the relative size of the TSZ.

4.2. Results using the size-effect model

The results from applying the size-effect data reduction method [5] to the peak loads of all three sizes of SE(B) specimens are presented in Table 3. For TSD series G and H, the peak loads for all three sizes of simulated SE(B) specimens could not be determined; therefore, the measured fracture toughness,  $K_{Ic}^{SZ}$ , for these series could not be obtained using the size-effect data reduction method. For TSD series I and J, the TSZ size was on the order of the node spacing in the simulations. This resulted in increased inaccuracy of the measured peak loads. When the peak loads were used with the size-effect data reduction method, the

Table 3  
Results from applying the size-effect data reduction method to simulated results from three sizes of SE(B) specimens using a variety of TSDs

TSD series	$K_{Ic}^{coh}$ input (MPa $\sqrt{m}$ )	$K_{Ic}^{SZ}$ (MPa $\sqrt{m}$ )	Difference percentage (Eq. (14))	Relative length of TSZ (%) (Eq. (15))
A	1.10	0.77	-30	20–40
B	<b>1.10</b>	<b>1.08</b>	-2	<b>40–50</b>
C	<b>1.10</b>	<b>1.18</b>	7	<b>30–50</b>
D	<b>1.10</b>	<b>1.21</b>	10	<b>30–50</b>
E	4.40	3.03	-31	60–75
F	4.40	2.03	-54	60–75
G	4.40	–	–	$\geq 75$
H	4.40	–	–	$\geq 75$
I	1.10	–	–	10
J	1.10	–	–	10–20
K	<b>1.10</b>	<b>1.22</b>	11	<b>10</b>
L	<b>1.10</b>	<b>1.12</b>	2	<b>10</b>
M	4.40	3.04	-31	20–40
N	<b>4.40</b>	<b>4.47</b>	2	<b>40–50</b>
O	<b>4.40</b>	<b>4.74</b>	8	<b>30–50</b>
P	<b>4.40</b>	<b>4.91</b>	12	<b>30–50</b>
Q	2.75	2.51	-9	30–50

Bold entries denote a difference percentage within 15%.

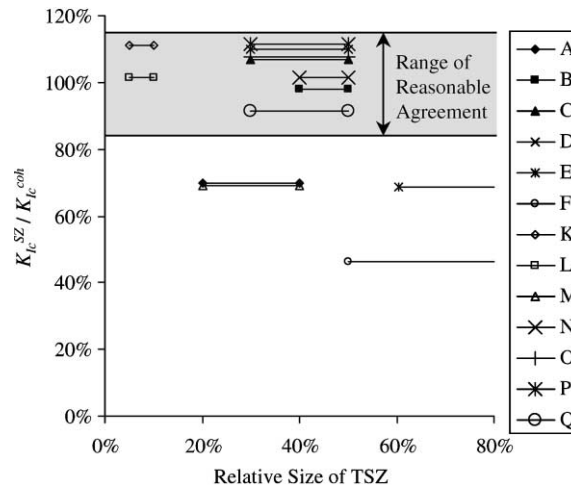


Fig. 12. Plot of the ratio of measured fracture toughness using the size-effect data reduction method to cohesive fracture toughness as a function of the range of relative sizes of the TSZ.

inaccuracies were amplified to a point where the  $K_{Ic}^{SZ}$  values were 3.96 and 1.68 MPa  $\sqrt{m}$ , respectively. These  $K_{Ic}^{SZ}$  values are probably unreasonably inaccurate and are not included in Table 3.

The objective of comparing the size-effect and fictitious crack models is to determine whether they predict the same behavior of a concrete structure at the scale of laboratory specimens for some range of cohesive zone property values. Again, the authors chose to quantify the difference in fracture toughness values required to make the same behavior prediction. The comparison of fracture toughness values was calculated using Eq. (14). Agreement between the fracture toughness values within 15% is considered reasonable, and those TSD's that produce reasonable agreement are highlighted in Table 3. Since many of the TSD's produce reasonable agreement of fracture toughness values, there is a significant range of concretes considered in this study for which the size-effect and fictitious crack models make reasonably similar predictions of the behavior of laboratory size structures using the same fracture toughness value in each model.

The data reduction method produces one fracture toughness value for the three sizes of specimens used; therefore, a range of relative sizes of the TSZ is associated with each result. The ranges are summarized from the individual values from Table 2. The ratio of measured fracture toughness to cohesive fracture toughness,  $K_{Ic}^{SZ}/K_{Ic}^{coh}$ , is compared to the range of TSZ percentages lengths in Fig. 12.

## 5. Conclusions

The results of this investigation confirm that, if the three models must predict the same behavior for infinitely large structures, they do not always predict the same behavior in structures at the size of laboratory test specimens. However, there are ranges of tension softening properties for which the three models *do* agree at the size of laboratory test specimens. Therefore, the three models might be used interchangeably for predicting structural behavior of average size structure members made of concretes developed in the future, if the tension softening properties of these concretes are in these ranges. As the tensile capacity of the concrete in the TSZ increases, the agreement of the models improved even if the fracture toughness is also increased.

The two-parameter data reduction method assumes that the TSZ is sufficiently small at peak load that the behavior of the specimen can be expressed in terms of an effectively longer crack experiencing LEFM

conditions. From the simulation results in this study, it appears that the relative size of the TSZ must be less than approximately 15% of the ligament length for the two-parameter model to predict similar behavior as similar to the fictitious crack model.

The size-effect data reduction method assumes that the nominal strength–specimen size relationship for a material is unaffected by the relative size of the TSZ. The validity of this assumption is difficult to show through direct observation of the TSZ. However, when the measured  $K_{Ic}^{SZ}$  value is within a few percent of  $K_{Ic}^{coh}$ , the assumption must be satisfied. From the various simulation results in this study, it appears that the total relative size of the TSZ at peak load is *not* an indication of how similar predictions of behavior will be from the size-effect and fictitious crack models. The appropriate guideline should probably be based upon the relative TSZ size considering only the initial softening portion of the TSD. Note, however, that the size-effect and fictitious crack models produce similar predictions of behavior for a broader range of TSZ properties than do the two-parameter and fictitious crack models.

## Acknowledgements

This research has been made possible through grants by the National Science Foundation, grant # CMS-9414243, and the Alcoa Foundation, and through the use of the high-performance computing facilities at the Cornell Theory Center.

## References

- [1] Bazant ZP, Pfeiffer PA. Determination of fracture energy from size effect and brittleness number. *ACI Mater J* 1987;84(6):463–80.
- [2] Jenq YS, Shah SP. A fracture toughness criterion for concrete. *Engng Fract Mech* 1985;21(5):1055–69.
- [3] Hillerborg A, Modeer M, Petersson P-E. Analysis of crack formation and crack growth in concrete by means of fracture mechanics and finite elements. *Cem Concr Res* 1976;6:773–82.
- [4] Elices M, Planas J. Size effect and experimental validation of fracture models. In: Elfgren L, Shah SP, editors. *Analysis of concrete structures by fracture mechanics*. Chapman & Hall; 1991. p. 99–127.
- [5] RILEM. Size-effect method for determining fracture energy and process zone size of concrete. *Mater Struct* 1990;23:461–5.
- [6] RILEM. Determination of fracture parameters ( $K_{Ic}^S$  and  $CTOD_c$ ) of plain concrete using three-point bend tests. *Mater Struct* 1990;23:457–60.
- [7] Martha LF, Gray LJ, Ingraffea AR. Three-dimensional fracture simulation with a single-domain, direct boundary element formulation. *Int J Numer Meth Engng* 1992;35:1907–21.
- [8] Bittencourt TN, Ingraffea AR. Three-dimensional cohesive crack analysis of short-rod specimens. In: Erdogan F, editor. *Fatigue and fracture mechanics*. ASTM STP 1220, vol. 25. American Society for Testing and Materials; 1995. p. 46–60.
- [9] Sousa JL. Three-dimensional simulation of near-wellbore phenomena related to hydraulic fracturing from a perforated wellbore. PhD dissertation. Department of Civil and Environmental Engineering: Cornell University, 1992.
- [10] Hanson JH. An experimental-computational evaluation of the accuracy of fracture toughness tests on concrete. PhD dissertation. School of Civil and Environmental Engineering: Cornell University, 2000.
- [11] Petersson P-E. Crack growth and development of fracture zones in plain concrete and similar materials. Report TVBM-1006/1-174. Division of Building Materials: Lund Institute of Technology, 1981.
- [12] Yankelevsky DZ, Reinhardt HW. Uniaxial behavior of concrete in cyclic tension. *J Struct Engng* 1989;115(1):166–82.
- [13] Swartz SE, Go CG. Validity of compliance calibration to cracked concrete beams in bending. *Exp Mech* 1984;24(2):129–34.
- [14] Bazant ZP. Size effect in blunt fracture: concrete, rock, metal. *J Engng Mech* 1984;110(4):518–35.
- [15] Rokugo H, Iwasa M, Suzuki T, Koyanagi W. Testing methods to determine tensile strain softening curve and fracture energy of concrete. In: Mihashi H, Takahashi H, Wittmann FH, editors. *Fracture toughness and fracture energy: test methods for concrete and rock*. Balkema; 1989. p. 153–63.
- [16] Kitsutaka Y, Kamimura K, Nakamura S. Evaluation of aggregate properties on tension softening behavior of high-strength concrete. In: Malhotra VM, editor. *High-performance concrete, SP-149*. American Concrete Institute; 1994. p. 711–27.
- [17] Gopalratnam VS, Shah SP. Softening response of plain concrete in direct tension. *J Am Concr Inst* 1985;82(3):310–23.
- [18] Montgomery DC. *Design and analysis of experiments*. New York: John Wiley & Sons; 2001.